

It's a gas: Oxidative dehydrogenation of propane over boron nitride catalysts

Peter Kraus^{a*}, R. Peter Lindstedt^b

a) School of Molecular and Life Sciences,
Curtin University,
GPO Box U1987, Perth 6845, WA

b) Department of Mechanical Engineering,
Imperial College London,
Exhibition Road, London SW7 2AZ

1 Abstract

Boron nitride and related boron-containing materials have recently been suggested as very promising catalysts in the oxidative dehydrogenation of propane. The high selectivity towards propylene at comparably high conversion significantly exceeds the performance of established vanadium-based catalysts. In the current work we show that the high selectivity towards propylene and ethylene is fully consistent with a gas-phase conversion mechanism and that it can be modelled reasonably well by the recent detailed microkinetic reaction mechanism of Hashemi and coworkers. Our analysis, using six heterogeneous catalytic reaction pathways, each representing a hypothetical limit case, shows that the boron nitride catalyst is responsible for initiating the gas-phase chemistry. The increased conversion of propane in cases with water co-feed, as well as the trends in the selectivities of minor species upon dilution of the catalytic bed and upon varying the C_3H_8/O_2 inlet ratio, as observed by Venegas and Hermans, are here explained as gas-phase phenomena. Hence, the oxidative dehydrogenation of propane over boron nitride catalysts is an example of a coupled gas- and catalytic- chemistry system. The current work also highlights the importance of modelling of the complete heated zone, including the rear heat shields and reactor padding if present.

16 1 Introduction

“It is surprising that boron nitride (BN), a material known for its high stability under oxidative conditions, is catalytically active at all.”^[1] Since this landmark 2016 publication by Grant et al.^[1] in Science, boron-containing materials have become a hot topic in oxidative dehydrogenation (ODH), and with

*E-mail: peter.kraus@curtin.edu.au

20 good reason. The claimed selectivity to propylene ($S(\text{C}_3\text{H}_6)$) is 80% at propane conversion ($X(\text{C}_3\text{H}_8)$)
21 of 21%,^[2] while established vanadium-based catalysts offer only 60% selectivity at half the conversion.^[1,3]
22 The performance of some BN materials remains stable up to 300 hours on stream^[2] and catalysts can
23 be regenerated by co-feeding NH_3 .^[4] In fact, it seems good ODH performance can be obtained with any
24 material provided it contains boron.^[5,6]

25 Most studies of ODH of alkanes over BN focus on the catalytic surface chemistry, and despite the
26 high temperatures required, usually in excess of 500°C , the potential contribution of gas-phase chemistry
27 remains comparably unassessed. This is understandable as blank experiments with SiO_2 instead of BN in
28 the reactor show almost no conversion.^[4,7] However, the operating conditions across the various catalytic
29 tests have not been standardised,^[8] making comparisons between datasets difficult. Pretreatment, heat
30 transport, diluent and dilution, reactor dimensions, and feed composition all play a significant role in
31 the activity of hexagonal boron nitride (hBN).^[6,8,9] Venegas et al. proposed that the observed catalytic
32 activity of diluted hBN for ODH of propane may be rooted in gas-phase oxidation chemistry, initiated
33 by catalytic surface reactions, and that hBN may even act as a radical quenching agent.^[8] This was
34 later reinforced by the suggestion that the role of the gas-phase must be established and incorporated
35 in future model development^[6]. Such mechanisms have been proposed for ODH of butane^[10] and more
36 recently propane.^[9]

37 It is a fortunate coincidence that a “low-temperature” (from a combustion point of view) gas phase
38 mechanism for propane oxidation has been recently published.^[11] This allows us to investigate the
39 relative gas-phase and catalytic contributions to the observed ODH of propane. We accordingly explore
40 the differences between the predicted gas-phase behaviour and observed catalytic performance under
41 dry conditions^[8] by coupling six catalytic “limit” mechanisms, derived from literature, to the gas-phase
42 chemistry of Hashemi et al.^[11] We emphasise the heterogeneous mechanisms used in this work are not
43 designed to represent the true surface chemistry of hBN. Rather, they are used as a probe to investigate
44 the limits of the impacts of the heterogeneous chemistry on the overall ODH process. These mechanisms
45 include direct dissociative adsorption as well as oxygen-mediated Eley-Rideal adsorption pathways, and
46 investigate the potential impact of catalytically-generated propylene, propoxy radicals, propyl radicals,
47 or C–C scission products on the gas-phase chemistry. The mechanisms are evaluated against the reference
48 experimental conditions that span a range of residence times and consider the impact of dilution of the

49 catalyst in dry feed^[8] with the impact of steam and O₂ concentration in the feed thoroughly evaluated
50 by Venegas et al.^[9]

51 **2 Computational methods**

52 The gas-phase and heterogeneous modelling in this work was performed using Cantera version 2.4.^[12]
53 All fitting is performed with the nonlinear least squares routine `curve_fit` from the `scipy.optimize`
54 Python library. The inputs used in the modelling, the resulting data, and the post-processing routines
55 are all included in the Binder-compatible Supporting Information archive.

56 **2.1 Gas-phase chemistry**

57 The following gas-phase models are used in this work: i) the “DTU” model developed for high-pressure
58 oxidation of propane,^[11] ii) the mechanism of Burluka et al. developed to model laminar burning
59 velocities of C₃ oxygenated species,^[13] and iii) the “JetSurF” mechanism developed for high-temperature
60 combustion of jet fuel surrogate mixtures.^[14] The DTU model includes low-temperature chemistry of
61 the hydroperoxyalkyl (QOOH) radicals,^[15] as well as revised C₃H₈ thermal activation^[16] and radical
62 abstraction^[11,17] rates. The Burluka model predates this low-temperature QOOH chemistry, but it
63 includes more complete decomposition pathways of propylene oxide (c-C₃H₆O) which we show to be a
64 potentially significant minor product. Finally, JetSurF is based on a C₁–C₄ submechanism^[18] that was
65 extensively validated for higher temperatures and is mainly included for comparison purposes.

66 The ignition delay and selectivity-vs-conversion plots shown in Section 3 are modelled using an
67 adiabatic constant pressure reactor, with the size of the time step adjusted dynamically by the solver.
68 The ignition point τ is determined as the time corresponding to the maximum in the time derivative
69 of the OH concentration ($\tau = \arg \max f(t) := d[\text{OH}]/dt$). At the current temperatures, propane
70 autoignition proceeds in two stages, with the first stage due to a combination of HO₂ and OH radical
71 chemistry, and the second, high-temperature ignition stage characterised by OH chemistry.^[19] The τ
72 determined using the above method corresponds to the latter, high-temperature ignition delay, and
73 therefore corresponds to an upper boundary.

74 **2.2 Catalytic surface chemistry**

Table 1: The catalytic H/O sub-mechanism^[20] in the form $AT^\beta e^{-E_A/RT}$, where $\theta(X)$ is surface fraction of species X , s_0 is the sticking coefficient, s indicates a surface bond and \dagger a first order rate law.

#	Reaction	A (m, mol, s)	β (-)	E_A (kJ/mol)
R1	$\text{H}_2 + 2^\dagger\text{Bs} \rightarrow 2\text{Hs}$	4.46×10^4	0.5	0
R2	$2\text{Hs} \rightarrow \text{H}_2 + 2\text{Bs}$	3.7×10^{15}	0	$67.4 - 6 \times \theta(\text{Hs})$
R3	$\text{H} + \text{Bs} \rightarrow \text{Hs}$	$s_0 = 1$	0	0
R4	$\text{O}_2 + 2\text{Bs} \rightarrow 2\text{Os}$	1.8×10^9	-0.5	0
R5	$\text{O}_2 + 2\text{Bs} \rightarrow 2\text{Os}$	$s_0 = 0.023$	0	0
R6	$2\text{Os} \rightarrow \text{O}_2 + 2\text{Bs}$	3.7×10^{15}	0	$213.2 - 60 \times \theta(\text{Os})$
R7	$\text{O} + \text{Bs} \rightarrow \text{Os}$	$s_0 = 1$	0	0
R8	$\text{H}_2\text{O} + \text{Bs} \rightarrow \text{H}_2\text{Os}$	$s_0 = 0.75$	0	0
R9	$\text{H}_2\text{Os} \rightarrow \text{H}_2\text{O} + \text{Bs}$	1×10^{13}	0	40.3
R10	$\text{OH} + \text{Bs} \rightarrow \text{OHs}$	$s_0 = 1$	0	0
R11	$\text{OHs} \rightarrow \text{OH} + \text{Bs}$	1×10^{13}	0	192.8
R12	$\text{Hs} + \text{Os} \leftrightarrow \text{OHs} + \text{Bs}$	3.7×10^{15}	0	11.5
R13	$\text{Hs} + \text{OHs} \leftrightarrow \text{H}_2\text{Os} + \text{Bs}$	3.7×10^{15}	0	17.4
R14	$\text{OHs} + \text{OHs} \leftrightarrow \text{H}_2\text{Os} + \text{Os}$	3.7×10^{15}	0	48.2

75 The heterogeneous models used in this work are based on the H/O sub-mechanism developed for CH₄
76 oxidation over platinum.^[20] The model comprises 14 reactions and thermochemistry, shown in Table 1.
77 We do not suggest that this H/O sub-mechanism developed for Pt is directly transferrable to hBN. For
78 instance, there are large differences in the dominant mode of O₂ adsorption, as on transition metals
79 the adsorption is dissociative,^[20] while on boron-containing materials the associative adsorption plays
80 an important role.^[7,21] The contribution of the hBN surface and the nature of the active site remains
81 a subject of intense study, with recent spectroscopic evidence of a significantly higher degree of surface
82 oxidation^[22,23] than previously thought. It has been proposed that the exceptional properties of boron-
83 containing materials are due to this dynamic layer, formed in situ under ODH conditions, as it features
84 active configurations that are not present in stable isomers.^[24] However, in the absence of an existing
85 validated H/O mechanism for hBN, our choice is one of convenience as the selected mechanism is
86 distributed with Cantera, and it is computationally efficient due to its small size. The impact of the
87 H/O sub-mechanism in the current work is also limited by ensuring the adsorption of propane is the
88 rate limiting step, as discussed below. Most pre-exponential factors in the H/O model are order-
89 of-magnitude estimates (10^{13} s^{-1} for desorptions and $3.7 \times 10^{15} \text{ m}^3\text{mol}^{-1}\text{s}^{-1}$ for bimolecular surface
90 reactions). All original parameters are retained with the site density adjusted to reproduce the conversion

91 observed with the current hBN based catalyst. The sensitivities to the site density (Γ) and oxygen
 92 adsorption parameters are accordingly assessed below. The thermochemistry of additional surface species
 93 is estimated from the corresponding gas-phase species in the DTU mechanism without further correction.
 94 In our previous work on Pt and Rh, the thermochemistry of the surface species was corrected by
 95 the heat of adsorption of the gas-phase species, obtained from systematic semi-empirical estimates.^[25]
 96 Similar corrections for hBN would require values for the atomic heats of adsorption, which are currently
 97 unavailable and would have to be estimated. As a result, we introduced irreversible catalytic reaction
 98 steps (i.e. separate forward and reverse reactions) for the $C_3/C_2/C_1$ surface chemistry.

Table 2: Properties of materials used in the heterogeneous model, where κ is the thermal conductivity, ρ the density and S_A the surface area.

	κ ($\text{W m}^{-1}\text{K}^{-1}$)	ρ (kg m^{-3})	S_A (m^2kg^{-1})
SiO ₂	3 ^[26]	100	1000
hBN	33 ^[8]	410 ^[8]	7000 ^[8]
SiC	300 ^[27]	860 ^[28]	13000 ^[28]

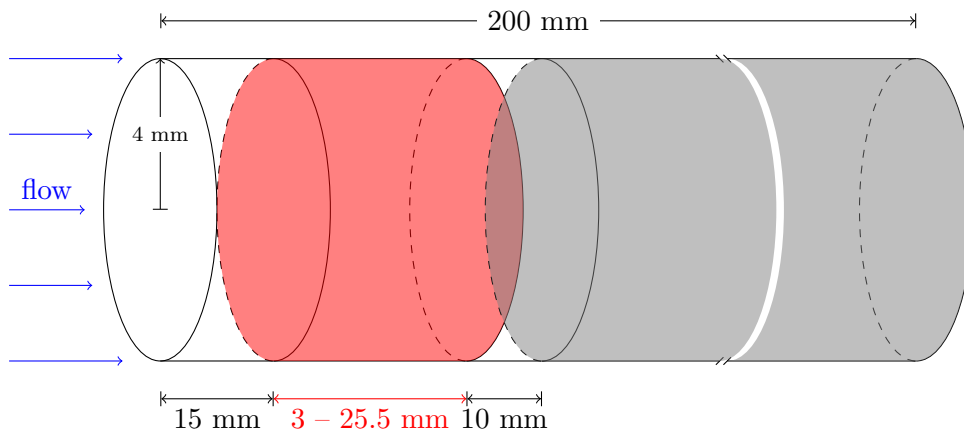


Figure 1: Schematic of the modelled reactor (not to scale). The catalytic section shown in red, front and rear heat shield sections filled with SiO₂-wool in white, and reactor padding SiO₂ chips in gray.

99 The catalytic reactor is modelled using a plug flow approximation, with the modelled domain com-
 100 prising four sections shown in Fig. 1: a SiO₂-wool heat shield, a catalytic section filled with hBN or
 101 optionally diluted with SiC, another SiO₂-wool heat shield, and the remainder of the reactor filled with
 102 SiO₂ chips. The applied boundary conditions are taken from Venegas and Hermans where available:^[8]
 103 an inlet temperature of 298 K; bath temperature of 773 K; reactor radius r of 4 mm; the tortuosity
 104 of the catalytic and SiO₂-wool sections set to 4; a porosity of the catalytic and SiO₂-wool sections of

105 0.4; inlet flow rates between 40 and 160 ml min⁻¹; length of the front and rear SiO₂-wool sections of 15
 106 and 10 mm, respectively; length of the catalytic section between 3 and 25.5 mm depending on dilution
 107 of hBN with SiC; an overall reactor length of 200 mm. The inlet composition is 30% C₃H₈, 15% O₂,
 108 and 55% N₂ by volume in all cases. The porosity and tortuosity of the section containing SiO₂ chips
 109 is not provided; for simplicity we assume a tortuosity of 1 with the impact of porosity on conversion
 110 assessed below. The temperature of the modelled reactor is regulated by an isothermal bath coupled
 111 to the domain using a $d = 4$ mm thick wall with material dependent properties listed in Table 2. The
 112 thermal conductances U_i for each reactor section i filled with material X are calculated according to
 113 Eq. (1), where V_i is the volume of the i th section.

$$U_i = \kappa_i(\mathbf{X}) \times d / (V_i S_{A_i}(\mathbf{X}) \rho_i(\mathbf{X})) \quad (1)$$

$$A_{c_i} = V_i S_{A_i}(\text{hBN}) \rho_i(\text{hBN}) / f_{\text{dil}} \quad (2)$$

114 The gas-phase chemistry is evaluated in all parts of the reactor with the heterogeneous mechanism
 115 enabled only in the catalytic section. In cases where hBN is diluted by SiC, the catalytic area of each
 116 cell A_{c_i} is scaled by the dilution factor $f_{\text{dil}} = V_{\text{bed}} / V_{\text{cat}} \in \{1.0, 1.5, 2.0, 3.5, 6.0, 8.5\}$ (see Eq. (2)), and
 117 the thermal conductance is approximated as the weighted sum of the conductivities of hBN and SiC.
 118 The density of grid points i in the four sections of the modelled reactor is 10/mm for the front and rear
 119 SiO₂-wool sections, 50/mm for the hBN-containing section, and 1/mm for the section filled with SiO₂
 120 chips. Grid resolution independence was confirmed using a 10× finer grid with the conversion converged
 121 to within 6% and selectivities to within 1% for the two grids. The carbon-based selectivities S and
 122 propane conversions X reported in this work are product based, using Eqs. (3) and (4), respectively.

$$S(\text{prod}) = \frac{n_{\text{C}}(\text{prod})x(i, \text{prod})f_e(i)}{\sum_{\mathbf{p} \neq \text{C}_3\text{H}_8} n_{\text{C}}(\mathbf{p})x(i, \mathbf{p})f_e(i)} \quad (3)$$

$$X(\text{C}_3\text{H}_8) = \frac{\sum_{\mathbf{p} \neq \text{C}_3\text{H}_8} n_{\text{C}}(\mathbf{p})x(i, \mathbf{p})f_e(i)}{\sum_{\mathbf{r}} n_{\text{C}}(\mathbf{r})x(i, \mathbf{r})f_e(i)} \quad (4)$$

123 Here, $n_{\text{C}}(\mathbf{p})$ is number of carbon atoms in species \mathbf{p} , $x(i, \mathbf{p})$ is the mole fraction of \mathbf{p} in cell i , and $f_e(i)$ is

124 the expansion factor defined as $f_e(i) = x(i, N_2)/x(0, N_2)$. Note that the index \mathbf{p} runs over the products
125 only, while the index \mathbf{r} runs over all species.

126 **3 Results and discussion**

127 To provide background for the aspects of the catalytic chemistry in the studied system, we first investi-
128 gate the behaviour of the gas-phase chemistry as predicted by the DTU,^[11] Burluka,^[13] and JetSurF^[14]
129 reaction mechanisms under the experimental conditions. Then, we assess the impact of the surface chem-
130 istry of hBN on the selectivity of the overall system by using six hypothetical limiting heterogeneous
131 reaction mechanisms. These limit mechanisms are used to probe the extremes of catalytic behaviour
132 in the context of the gas-phase chemistry, by imposing 100% catalytic selectivity towards either propy-
133 lene, propoxy radicals, propyl radicals, or C–C scission products. We then explore the contribution
134 of the gas-phase chemistry within these limits of possible catalytic behaviours and the experimentally
135 observed conversion and selectivities.^[8] Finally, we briefly discuss more recent experiments where the
136 inlet composition was varied.^[9]

137 **3.1 Gas-phase selectivities to major products**

138 The temperatures used in most investigations of propane ODH over hBN are usually in excess of 500°C,
139 which is higher than the usual conditions applied with vanadium-based catalysts.^[3] Such temperatures
140 are potentially compatible with gas-phase ignition. Despite this, the contribution of gas-phase chemistry
141 to the performance of hBN has not been quantified. Control experiments performed using a reactor filled
142 only with quartz chips have been reported and show “negligible” conversion at well below 1%.^[8] While
143 conceptual catalytic and combined homo- and heterogeneous mechanisms have been proposed,^[1,7–10]
144 only two studies have assessed the gas-phase behaviour: i) Loiland et al. applied a gas-phase microki-
145 netic model (AramcoMech2.0) to study gas-phase effects, however, the imposed boundary conditions (a
146 100 mm long modelled section) appear incongruous with the geometry of the experimental reactor (38 mm
147 long diluted catalytic bed in a 610 mm long heated quartz reactor).^[29] ii) Venegas et al. performed a
148 chemical kinetic analysis using a combined gas-phase and heterogeneous reaction mechanism, however,
149 only selected gas-phase pathways were coupled to the surface chemistry instead of a comprehensive

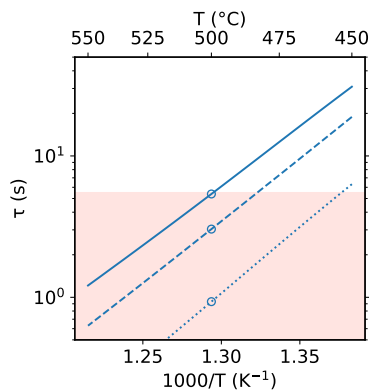


Figure 2: High temperature adiabatic ignition delay times (τ) based on the OH radical profile for a 15% O₂, 30% C₃H₈, 55% N₂ mixture as a function of the initial temperature at atmospheric pressure. The DTU mechanism (—) is compared to the Burluka (.....) and JetSurF (---) mechanisms. The red area indicates τ for the reactor in the experiments of Venegas and Hermans.^[8] Circles highlight a temperature of 500°C.

151 The high temperature ignition delays shown in Fig. 2 present an indication that gas-phase phenomena
 152 may play a non-negligible role under the studied conditions. At 500°C, the DTU mechanism (—) shows
 153 an ignition delay just outside the residence time domain in the experiments of Venegas and Hermans^[8]
 154 (red zone); the other two mechanisms (Burluka (.....) and JetSurF (---)) predict ignition well within
 155 the experimental time domain. It should further be noted that the HO₂ radical chemistry will be
 156 active in the gas phase at lower temperatures. The experimental temperature of 500°C is determined
 157 from a single thermocouple embedded in the catalytic bed,^[8] and despite best practices ensuring the
 158 bed is as isothermal as practicable, small inhomogeneities from the reaction temperature would have an
 159 exponential effect on the kinetics this close to self-ignition. We note that the ignition delay times shown in
 160 Fig. 2 are obtained from adiabatic calculations, while the catalytic reactor is likely close to the isothermal
 161 limit. The temperature rise for the adiabatic computations is 3 K at 1% conversion and reaches an upper
 162 limit of 103 K at 20% conversion. The gas phase contribution is expected to be correspondingly higher
 163 than observed experimentally. Therefore, further results from gas-phase calculations are presented as a
 164 function of conversion. For combined heterogeneous and gas-phase calculations, we model the reactor
 165 using a plug-flow approximation coupled to a heat bath, validated in Section 3.3 below.

166 The performance of hBN (and other B-containing materials) for ODH of propane is remarkable
 167 mainly due to the high selectivity to propylene and ethylene. However, as shown in Figure 3, the high

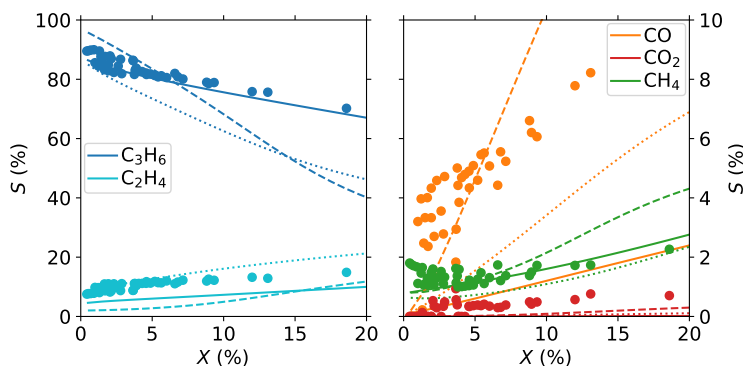


Figure 3: Selectivities (S) vs conversion (X) obtained exclusively from gas-phase kinetics. The DTU mechanism (—) is compared to the Burluka (⋯) and JetSurF (---) mechanisms and experimental data at all dilutions (●).^[8] The computations assume an adiabatic reactor with initial conditions of 500°C and atmospheric pressure, and a 15% O₂ / 30% C₃H₈ / 55% N₂ inlet composition.

168 selectivity to both propylene (C₃H₆, —) and ethylene (C₂H₄, —) is consistent with the kinetics of the
 169 DTU gas-phase mechanism. The experimental $S(\text{C}_3\text{H}_6)$ at $X(\text{C}_3\text{H}_8) \leq 20\%$ is matched almost exactly,
 170 while the trend in $S(\text{C}_2\text{H}_4)$ is predicted qualitatively with a constant underprediction of $\approx 5\%$ in the
 171 same conversion range. The other two mechanisms significantly underpredict the observed $S(\text{C}_3\text{H}_6)$. For
 172 minor products, methane (CH₄, ●) is well predicted by the DTU (—) and Burluka (⋯) mechanisms,
 173 but the main combustion product CO (---) is much better captured by JetSurF. The results indicate
 174 strongly that the pyrolysis part of the DTU mechanism is accurate while experimental selectivity to CO
 175 indicates that further low temperature oxidation pathways may be required.

176 3.2 Gas-phase selectivities to minor products

177 All three mechanisms underpredict the experimental $S(\text{CO}_2)$ by $\simeq 1\%$. The best agreement is obtained
 178 by JetSurF (--- in Fig. 3), which predicts roughly half this value. The DTU mechanism also predicts
 179 propylene oxide (c-C₃H₆O) to be a significant minor product with $S(\text{c-C}_3\text{H}_6\text{O})$ around 8%. However,
 180 propylene oxide was neither observed experimentally,^[8] nor predicted by Burluka and JetSurf mech-
 181 anisms. The DTU mechanism contains revised propylene oxide formation pathways passing via the
 182 QOOH route that are of particular relevance to the current temperature window.^[15] However, the asso-
 183 ciated destruction pathways have to date not been formulated. The Burluka and JetSurF mechanisms
 184 rely upon a simpler formation step via $\text{C}_3\text{H}_6 + \text{HO}_2 \leftrightarrow \text{c-C}_3\text{H}_6\text{O} + \text{OH}$, but include c-C₃H₆O destruc-
 185 tion pathways via ring opening towards acetone (CH₃C(O)CH₃) and propionaldehyde (CH₃CH₂CHO).

186 Propylene oxide is a liquid at room temperature and pressure, and the reactor effluent is cooled to -5°C
 187 to remove water prior to the chromatographic analysis. Hence, propylene oxide may be inadvertently
 188 removed from the effluent stream. However, the reported error in the experimental carbon mass balance
 189 is 3%,^[8] significantly less than the amount of propylene oxide predicted by the DTU mechanism. In-
 190 clusion of decomposition pathways of propylene oxide should ultimately lead to increased CO_2 and CO
 191 production,^[30] and improved agreement with experimental data as discussed below. It may further be
 192 noted that the catalyst may be active to propylene oxide as noted for copper-based catalysts by Xiao
 193 and Wang.^[31]

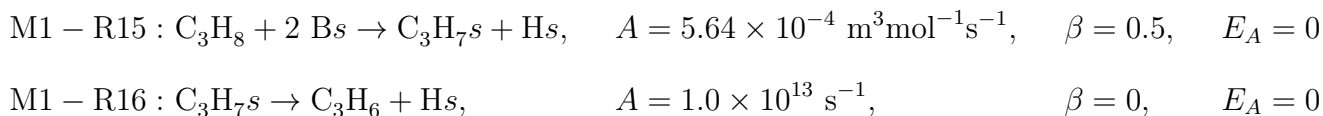
Table 3: The six heterogeneous “limit” submechanisms in the form $AT^{\beta} e^{-E_A/RT}$. † indicates rate fitted to obtain $X(\text{C}_3\text{H}_8) = 3.65\%$ with $\Gamma = 1.6 \times 10^{-7} \text{ mol m}^{-2}$ and 20% porosity with undiluted catalyst at 40 ml min^{-1} flow.

#	Reaction	A (m, mol, s)	β (-)	E_A (kJ/mol)
M1-R15	$\text{C}_3\text{H}_8 + 2 \text{Bs} \rightarrow \text{C}_3\text{H}_7\text{s} + \text{Hs}$	† 5.64×10^{-4}	0.5	0
M1-R16	$\text{C}_3\text{H}_7\text{s} \rightarrow \text{C}_3\text{H}_6 + \text{Hs}$	1×10^{13}	0	0
M2-R15	$\text{C}_3\text{H}_8 + 2 \text{Os} \rightarrow \text{C}_3\text{H}_7\text{Os} + \text{OHs}$	† 4.61×10^{-7}	0.5	0
M2-R16	$\text{C}_3\text{H}_7\text{Os} \rightarrow \text{C}_3\text{H}_6 + \text{OHs}$	1×10^{13}	0	0
M3-R15	$\text{C}_3\text{H}_8 + 2 \text{Os} \rightarrow \text{C}_3\text{H}_7\text{Os} + \text{OHs}$	† 2.79×10^{-7}	0.5	0
M3-R16i	$\text{C}_3\text{H}_7\text{Os} \rightarrow \text{i-C}_3\text{H}_7\text{O} + \text{Bs}$	2×10^{13}	0	20.9
M3-R16n	$\text{C}_3\text{H}_7\text{Os} \rightarrow \text{n-C}_3\text{H}_7\text{O} + \text{Bs}$	6×10^{13}	0	3.4
M4-R15	$\text{C}_3\text{H}_8 + 2 \text{Bs} \rightarrow \text{C}_3\text{H}_7\text{s} + \text{Hs}$	† 3.81×10^{-4}	0.5	0
M4-R16i	$\text{C}_3\text{H}_7\text{s} \rightarrow \text{i-C}_3\text{H}_7 + \text{Bs}$	2×10^{13}	0	31.4
M4-R16n	$\text{C}_3\text{H}_7\text{s} \rightarrow \text{n-C}_3\text{H}_7 + \text{Bs}$	6×10^{13}	0	20.9
M5-R15	$\text{C}_3\text{H}_8 + 2 \text{Os} \rightarrow \text{C}_3\text{H}_7\text{Os} + \text{OHs}$	† 2.65×10^{-7}	0.5	0
M5-R16	$\text{C}_3\text{H}_7\text{Os} \rightarrow \text{C}_2\text{H}_4 + \text{CH}_3 + \text{Os}$	1×10^{13}	0	0
M6-R15	$\text{C}_3\text{H}_8 + 2 \text{Os} \rightarrow \text{C}_3\text{H}_7\text{Os} + \text{OHs}$	† 4.74×10^{-7}	0.5	0
M6-R16	$\text{C}_3\text{H}_7\text{Os} \rightarrow \text{C}_2\text{H}_6 + \text{CO} + \text{Bs}$	1×10^{13}	0	0

194 3.3 Catalysis in the propylene forming limit (M1)

195 The six heterogeneous “limit” submechanisms are shown in Table 3. The first of these sequences (M1)
 196 is used to evaluate the impact of catalytic formation of propylene on the selectivities, as well as validate
 197 configuration related parameters such as the reactor porosity and the catalytic site density. The mor-
 198 phology of the catalyst may impose transport limitations and therefore impact the observed outcomes.
 199 The global impact of different morphologies will be reflected in the residence time, as the tortuosity and
 200 porosity of the bed will differ. In previous work,^[25] we imposed mass transport limitations via efficiency
 201 factors and the same approach could be applied here (e.g. based on Knudsen diffusion). However, this

202 would further emphasise the effects of the gas phase chemistry. We instead choose to use the plug-flow
 203 model and apply the literature values of porosity and tortuosity^[8] in the first three reactor sections (see
 204 Fig. 1). To validate our plug-flow reactor model, we determine the impact of porosity of the last section
 205 on the overall conversion due to residence time effects in the heated section. For this purpose, the DTU
 206 gas-phase mechanism is coupled to the catalytic chemistry shown in Table 1 and extended by sequence
 207 M1 as shown below.



208 The desorption in M1-R16 is unlikely to be barrierless. However, setting a barrier height has no effect if
 209 M1-R16 is not rate limiting as there is no alternative outlet for $\text{C}_3\text{H}_7\text{s}$. Under such circumstances, the
 210 pre-exponential of M1-R15 can be fitted to match the observed conversion. The conversion reported in
 211 the control experiments without hBN is $X(\text{C}_3\text{H}_8) = 1\%$ at 550°C and 0.3% at 500°C ^[8] with the latter
 212 value indicated in Fig. 4 by the open circle (\circ). We note again that in the experiments, the temperature
 213 of the furnace is controlled by a single thermocouple embedded in the catalytic bed.^[8] This low level of
 214 conversion is only matched when the porosity of the rear section is around 1%, an unusually low value
 215 given that the porosity of the SiO_2 wool is 40%^[8] and the porosity of SiO_2 chips has been reported
 216 as high as 50%.^[32] In the following, we tentatively apply an intermediate value of porosity of 20%,
 217 corresponding to a conversion of 0.9% in the control experiment.

218 In addition to the porosity of the last section of the reactor and the adsorption rate constant M1-R15,
 219 $X(\text{C}_3\text{H}_8)$ is also a function of the site density Γ . The physical constraint on the site density of hBN is
 220 $\Gamma \leq 3.04 \times 10^{-5} \text{ mol m}^{-2}$, derived from a theoretical unit cell area of 5.462 \AA^2 per boron site.^[33] The
 221 Γ used throughout the current work is fitted together with the pre-exponential of M1-R15 to ensure
 222 $X(\text{C}_3\text{H}_8) = 3.65\%$ for the undiluted case, and 18.60% for $V_{\text{bed}}/V_{\text{cat}} = 8.5$, given a porosity of 20% in the
 223 last section of the reactor, shown in Fig. 4. The resulting values are $A_{\text{M1-R15}} = 5.64 \times 10^{-4} \text{ m}^3\text{mol}^{-1}\text{s}^{-1}$
 224 and $\Gamma = 1.6 \times 10^{-7} \text{ mol m}^{-2}$ corresponding to 0.5% availability of boron sites with respect to the
 225 theoretical maximum.

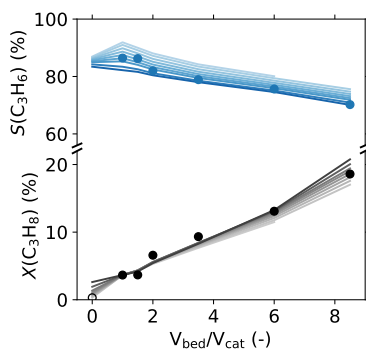


Figure 4: Effect of porosity on the propane conversion and propylene selectivity, with the pre-exponential of R15-1 fitted to match conversion for undiluted case. Shading implies porosity in the range of 1–50%. Γ set to $1.6 \times 10^{-7} \text{ mol m}^{-2}$ for all dilutions and porosities. Flow rate $\sim 40 \text{ ml min}^{-1}$.

226 The above two-step process is a limiting case. It is much more likely the actual propane activation
 227 process involves reversible C_3H_8 adsorption followed by a C–H bond activation on the surface with an
 228 appreciable barrier. The dissociative adsorption described by M1-R15 can accordingly be thought of
 229 as a global reaction step with an exceptionally low sticking coefficient ($s_0 \sim 10^{-12}$) when compared to
 230 $s_0 = 5.8 \times 10^{-3}$ for C_3H_8 on rhodium.^[34] To obtain the same rate constant at 500°C , assuming the same
 231 propane sticking coefficient as on rhodium, the dissociative adsorption would have to proceed with a
 232 barrier of 117 kJ/mol. The barrier appears high, but is well below the reported experimental apparent
 233 activation energies for ODH of propane (184–233 kJ/mol^[2,29]). For comparison, on vanadium oxides,
 234 dissociative adsorption of propane was calculated to proceed with a barrier of 144–151 kJ/mol.^[35]

235 3.4 Catalysis in the Eley-Rideal mediated propylene forming limit (M2)

236 The second (M2) limiting mechanism features an O_s -mediated Eley-Rideal type C_3H_6 forming mecha-
 237 nism as proposed by Shi et al.^[7]. The mechanism is consistent with the presence of surface oxygen in
 238 X-ray photoelectron spectra (XPS)^[1,5] as well as B–OH vibrations in infrared spectra.^[7,36] The applied
 239 rate constants are listed in Table 3. The adsorption rate (M2-R15) has again been fitted to match
 240 the conversion in the undiluted case, which allowed us to apply a barrierless desorption step, as the
 241 adsorption is rate limiting.

242 The direct C_3H_6 mechanism (M1, — in Fig. 5) and the O_s -mediated C_3H_6 mechanism (M2, not
 243 shown) show nearly identical selectivity and conversion profiles, despite the different nature of C_3H_8
 244 activation on the catalytic surface. The pre-exponentials of the adsorption steps in the two mechanisms

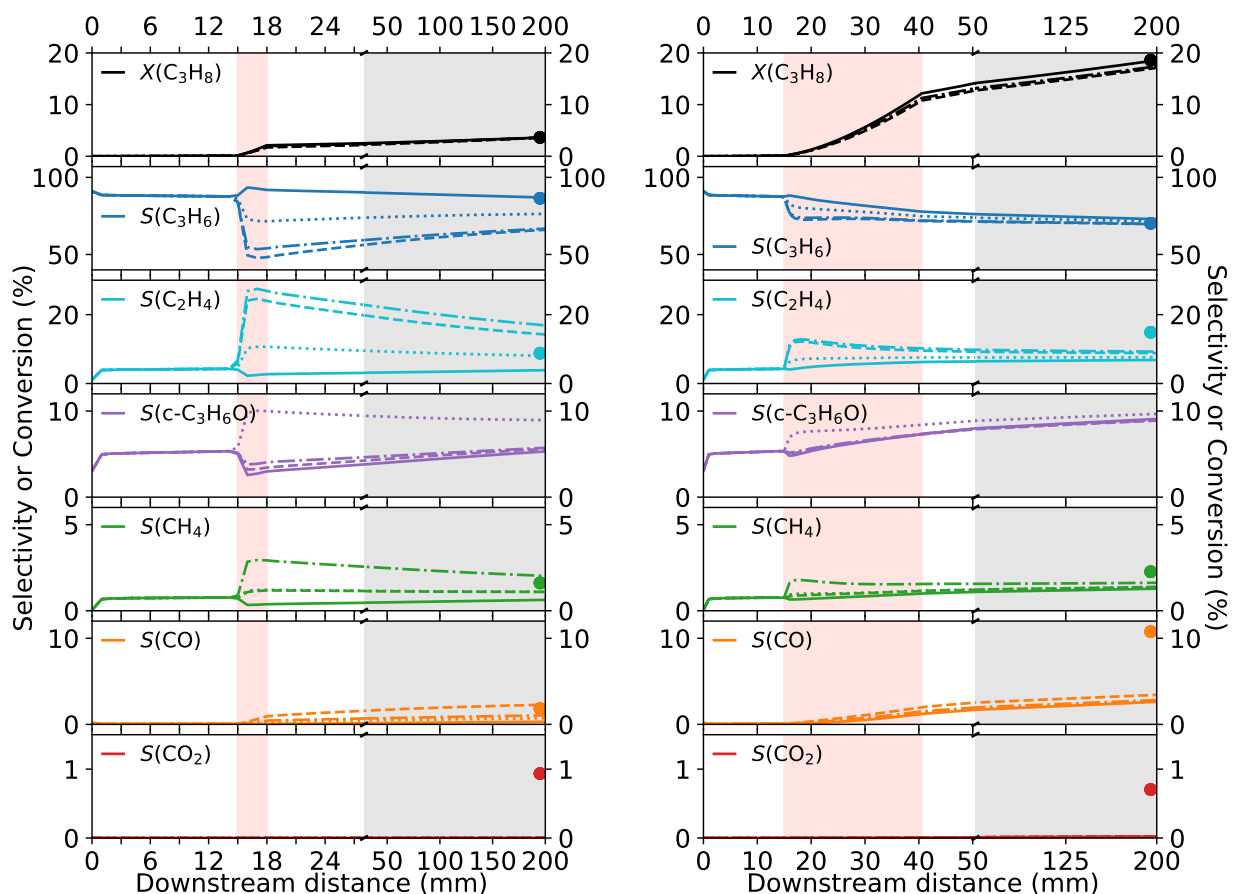


Figure 5: Selectivities (S) and conversion (X) of selected species as a function of downstream distance with four of the six limit mechanisms: M1: direct C_3H_6 (—), M3: O_s -mediated C_3H_7O (- - -), M4: direct C_3H_7 (.....), and M5: O_s -mediated C–C scission (- · - ·). Case with an undiluted catalyst (left) and with the highest dilution ($V_{bed}/V_{cat} = 8.5$, right), both at $\sim 40 \text{ ml min}^{-1}$. Lines are calculated data, circles are experimental results,^[8] shaded areas correspond to the front and rear heat shield (white), the catalytic zone (red), and SiO_2 chips (gray).

245 differ by around a factor of 10^3 with the O_s -mediated M2 mechanism being the more active (i.e. a
 246 reduction in the pre-exponential factor is required to meet the target conversion). The predicted surface
 247 coverages of B_s and O_s are 1.8% and 98.2% after the first mm and 2.8% and 97.1% after the last mm
 248 of the undiluted catalyst, respectively. When the effect of surface coverages on the rate laws is taken
 249 into account, the Eley-Rideal pathway leads to a $5/2$ faster propane adsorption rate at the beginning
 250 of the catalytic section. However, both mechanisms quickly converge to the same adsorption rate in
 251 the last mm of the catalyst, yielding indistinguishable conversion profiles. The availability of free (B_s)
 252 and O_s sites is therefore not limiting in the current model. A small proportion of sites (0.06% in
 253 undiluted, 0.1% in diluted cases) is covered by OH_s , regardless of the adsorption pathway. The presence

254 of OHs is consistent with analysis of the spent catalysts, but it is not conclusive proof of an Eley-Rideal
 255 mechanism, as the adsorption of propane may equally plausibly proceed on exposed Bs or Os sites,
 256 and the B–OH species can be explained by either abstraction of the second H by Os leading to C₃H₆
 257 formation, or by a surface reaction between Hs and Os. The predicted surface coverages may change
 258 once multiple branching pathways are introduced, and once the H/O submechanism is validated for
 259 hBN.

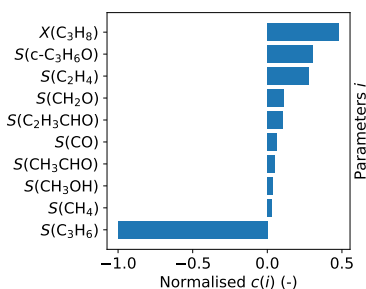


Figure 6: Normalised sensitivity coefficients $c(i)$ of parameters i with respect to the O₂ adsorption rate for reaction (R4) in the H/O submechanism from Deutschmann et al.^[20]

260 The H/O submechanism, developed for platinum, is taken verbatim from Deutschmann et al.^[20]
 261 As we have adjusted Γ , a sensitivity analysis on the rate of O₂ dissociative adsorption (R4) was per-
 262 formed by varying the pre-exponential factor (A_{R4}) by an order of magnitude between $1.8 \times 10^8 - 1.8 \times$
 263 $10^{10} \text{ m}^6\text{mol}^{-2}\text{s}^{-1}$. The largest absolute sensitivity coefficient is $c(S(\text{C}_3\text{H}_6)) = \partial S(\text{C}_3\text{H}_6, A_{R4})/\partial A_{R4}$ with
 264 value on the order of 10^{-2} , which indicates the H/O chemistry is significantly contributing to the sur-
 265 face chemistry. The normalised coefficients of the 10 most sensitive parameters are shown in Figure 6:
 266 $X(\text{C}_3\text{H}_8)$ and selectivities to minor species correlate positively with A_{R4} , while $S(\text{C}_3\text{H}_6)$ correlates neg-
 267 atively. In a rigorous approach to mechanism development, the H/O submechanism would have to be
 268 tailored to account for the differences between Pt and hBN, including pathways such as the associative
 269 adsorption of O₂,^[7] or the role H₂O may play in active site regeneration.^[9] Figure 6 shows that a further
 270 increase in the ratio of the effective sticking probabilities of O₂ and C₃H₆ would lead to a higher activity
 271 of the catalyst and lower selectivity to propylene.

272 As shown in Fig. 5, the M1 and M2 mechanisms are unsurprisingly the most selective towards
 273 C₃H₆ (—). The downstream profiles show only a small amount of post-catalytic combustion of the
 274 main product (gray shading). However, similarly to the gas-phase results, the selectivities towards

275 C_2H_4 (—) and CO (—) are underpredicted, especially in diluted catalytic beds ($\Delta \sim 8\%$). This
276 may be a consequence of the high selectivity towards propylene oxide ($c-C_3H_6O$, —, 9.0%), acrolein
277 (C_2H_3CHO , 3.3%) and formaldehyde (CH_2O , 1.9%), neither of which has been recorded experimentally.
278 When compared to the gas-phase S vs X results (Fig. 3), the addition of the surface pathways decreases
279 the agreement with experiment. Therefore, while C_3H_6 may be produced on the surface, it is unlikely
280 to be the only catalytic product as proposed by Shi et al.^[7]

281 3.5 Catalysis in the radical forming limit (M3 and M4)

282 The initially proposed mechanism for the activity of hBN (M3) involves adsorption on oxygen-covered
283 boron sites and leading to the formation of propoxy radicals (C_3H_7O).^[1] We also include the direct,
284 propyl radical (C_3H_7) forming analogue (M4), considered by Venegas and Hermans.^[8] A catalytic process
285 where propyl radicals desorb rather than undergo further H-abstraction to propylene on the surface
286 seems unlikely. Venegas et al.^[9] recently proposed a mechanism where surface-bound oxygen (Os)
287 abstracts hydrogen from propane leading to C_3H_7 isomers via a barrierless process. Here, we include the
288 propyl forming mechanism to probe the potential impact that additional propyl radicals would have on
289 the gas-phase behaviour. The rate constants are listed in Table 3. Rather than overfitting the models
290 by using six parameters in each of the two mechanisms, we have opted to fit only the adsorption pre-
291 exponential terms (M3-R15 and M4-R15) to match the observed conversion. The adsorption steps are
292 therefore rate limiting. The pre-exponential factors for the desorption step are branched to iso- and
293 n-propoxy (or propyl) radicals, and the order of magnitude estimates are scaled 2:6 to account for the
294 number of equivalent hydrogens in propane. The barrier heights for product desorption are taken from
295 similar gas-phase reactions in the DTU mechanism. As the reference experiments have been carried
296 out at a single temperature, and the adsorption step is enforced to be rate limiting, the choice of the
297 desorption barrier heights is arbitrary.

298 The two mechanisms show a very different behaviour when considered in isolation as well as when
299 compared to the propylene forming limit cases (M1 and M2). In the undiluted case, the propoxy
300 mechanism (---) results in a significantly higher amount of C–C scission than the propyl mechanism
301 (⋯⋯). The selectivity to the main product, propylene, is significantly underpredicted by both of these

302 mechanisms, and it is dropping in the catalytic zone (red area) of the reactor. The mechanism based
 303 on C_3H_7O isomers underpredicts $S(C_3H_6)$ by over 20% (---), while overpredicting $S(C_2H_4)$ by 6% (---
 304), and CO (---) by 0.6%. By contrast, in the undiluted case the mechanism featuring C_3H_7 isomers
 305 underpredicts $S(C_3H_6)$ to a smaller degree (.....), and it predicts the correct amount of C_2H_4 (.....).
 306 However, the selectivity to propylene oxide (.....) is nearly double that of the other mechanisms studied,
 307 as the propyl radicals are clearly forming propylene oxide in the gas-phase upon (the unlikely) desorption
 308 from the catalyst. Finally, upon dilution of the catalytic bed, both mechanisms converge towards the
 309 values predicted for the M1 and M2 mechanisms as the gas-phase chemistry pushes the selectivities
 310 towards equilibrium. Both mechanisms also predict $c-C_3H_6O$ and C_2H_3CHO selectivities similar to the
 311 M1 and M2 mechanisms, with the C_3H_7O pathways yielding the highest amount of CH_2O (2.8%).

312 3.6 Catalysis in the C–C scission limit (M5 and M6)

313 The final two limit mechanisms studied here are two-step models leading to either C_2H_4 and CH_3
 314 formation (M5), or C_2H_6 and CO formation (M6), both proceeding via Os -mediated adsorption, see
 315 Table 3. From the multitude of possible saturated, unsaturated, or oxygenated C–C scission products, we
 316 chose the above two combinations to directly stimulate C_2H_4 and CH_4 (M5) or CO (M6) production. We
 317 note that detailed heterogeneous microkinetic mechanisms for C_3 species that also include C_2 products
 318 are rather rare: the above mentioned mechanism for propane partial oxidation over rhodium^[34] only
 319 contains desorption pathways for C_3H_8 , CO, CO_2 , and CH_4 ; the mechanism for propane ODH over
 320 vanadium oxide catalysts is more complete^[35] but has, to our knowledge, not been evaluated together
 321 with gas-phase chemistry. As in previous cases, the rate constants of the adsorption processes (M5-R15,
 322 M6-R16) are fitted to match the experimental conversion and therefore are rate limiting.

323 When the surface chemistry is fully shifted towards C_2H_4 and CH_3 (M5, ---), the selectivities to
 324 $S(C_2H_4)$ (---) and $S(CH_4)$ (---) exceed the experimental values for the undiluted case. Tian et al.^[37]
 325 suggested a catalytic C–C scission would lead to a 1:1 $C_2:C_1$ distribution in products while a higher ratio
 326 of 2:1 is observed experimentally in the undiluted case.^[8] The authors proposed a catalytic CH_3 -coupling
 327 process as a way of accounting for this discrepancy.^[37] Here, we obtain an overall $C_2:C_1$ ratio of 1.67
 328 with the oxygen mediated C_3H_6 forming mechanism (M2) and ratios above 1.90 with both C–C scission

329 mechanisms. For the undiluted cases, catalytic C–C scission unsurprisingly leads to higher C₂:C₁ ratios
 330 than mechanisms without surface C–C bond scission. Contrary to previous reports,^[21,37] we show that
 331 the experimental C₂:C₁ ratios can be matched without CH₃-coupling surface reactions. In all other
 332 aspects, the C₂H₄ and CH₃ mechanism (M5) is very similar to the M3 mechanism corresponding to the
 333 i–C₃H₇O and n–C₃H₇O forming limit (---). On the other hand, the C₂H₆ and CO forming limit (M6,
 334 not shown) performs rather poorly, as $S(\text{C}_3\text{H}_6)$ is underpredicted by over 30%, $S(\text{CO})$ is overpredicted
 335 by 10%, and most of the 22% of C₂H₆ produced on the surface does not dehydrogenate towards C₂H₄
 336 in the gas phase. It is therefore unlikely that CO is formed via direct oxidation of C₃H₈ on the surface,
 337 or that C₂H₆ is formed by the catalyst.

338 Upon dilution of the catalytic bed, convergence of both C–C scission pathways with the other four
 339 mechanisms (M1-M4) can be observed, leading to a significant underprediction of selectivities to $S(\text{C}_2\text{H}_4)$
 340 (---, $\Delta = 5\%$) and $S(\text{CO})$ (---, $\Delta = 8\%$) even with C₂H₄ or CO formed catalytically on the surface.
 341 This behaviour is accompanied by a high selectivity to experimentally undetected products c–C₃H₆O,
 342 C₂H₃CHO and CH₂O.

343 3.7 Impact of propylene oxide chemistry on selectivities

344 As discussed above, the selectivity towards propylene oxide calculated with the DTU mechanism appears
 345 at variance with experimental data. The low temperature chemistry of propylene oxide is hence likely
 346 to require further work. By contrast, the propylene oxide chemistry in the JetSurF mechanism is based
 347 on the high temperature shock temperature work by Lifshitz and Tamburu^[38]. This mechanism was
 348 later expanded by Burluka et al.^[13] and the resulting c–C₃H₆O submechanism is listed in Table 4. We
 349 note that the c–C₃H₆O and C₂H₃CHO pathways are not directly coupled and inclusion of the high-
 350 temperature decomposition pathways into the DTU mechanism does not impact the selectivities at high
 351 bed dilutions. However, the conversion of propane goes down appreciably from 18.5% to 16.7%.

352 In view of the incomplete low temperature propylene oxide chemistry, a different approach is to
 353 replace the c–C₃H₆O pathways in the DTU mechanism with that shown in Table 4. This modified
 354 mechanism is denoted DTU/B. As shown in Fig. 7, the gas-phase selectivity to propylene oxide drops
 355 (---), and is compensated mainly by an increase in $S(\text{C}_3\text{H}_6)$ (---) and a small increase in $S(\text{CO})$

Table 4: Propylene oxide formation and decomposition pathways from Burluka et al.^[13] with rate parameters in the form $AT^\beta e^{-E_A/RT}$.

Reaction	A (m, mol, s)	β (-)	E_A (kJ/mol)
$C_3H_6 + HO_2 \leftrightarrow c-C_3H_6O + OH$	1.05×10^6	0.0	59.46
$C_3H_6 + CH_3OO \leftrightarrow c-C_3H_6O + CH_3O$	4.00×10^5	0.0	49.04
$CH_3CH_2OO + C_3H_6 \leftrightarrow cC_3H_6O + CH_3CH_2O$	8.05×10^5	0.0	67.78
$C_3H_6 + CH_2CHCH_2OO \leftrightarrow c-C_3H_6O + c-C_3H_5O$	1.05×10^5	0.0	59.41
$C_3H_6 + n-C_3H_7OO \leftrightarrow c-C_3H_6O + n-C_3H_7O$	1.05×10^1	0.0	0.0
$c-C_3H_6O \leftrightarrow C_2H_5 + HCO$	2.45×10^{13}	0.0	244.80
$c-C_3H_6O \leftrightarrow CH_3CH_2CHO$	1.82×10^{14}	0.0	244.80
$c-C_3H_6O \leftrightarrow CH_3 + CH_3CO$	4.54×10^{13}	0.0	250.60
$c-C_3H_6O \leftrightarrow CH_3 + CH_2CHO$	2.45×10^{13}	0.0	246.10
$c-C_3H_6O \leftrightarrow CH_3 + c-C_2H_3O$	8.00×10^{15}	0.0	384.97
$c-C_3H_6O + H \leftrightarrow H_2 + CH_2CO + CH_3$	2.70×10^1	2.0	20.92
$c-C_3H_6O + O \leftrightarrow OH + HCO + C_2H_4$	7.80×10^7	0.0	21.80
$c-C_3H_6O + OH \leftrightarrow H_2O + CH_2CO + CH_3$	7.80×10^0	2.0	-3.20
$c-C_3H_6O + HO_2 \leftrightarrow CH_2CO + CH_3 + H_2O_2$	1.20×10^6	0.0	64.85
$c-C_3H_6O + CH_3 \leftrightarrow CH_2CO + CH_3 + CH_4$	6.00×10^5	0.0	40.20
$c-C_3H_6O + CH_3OO \leftrightarrow CH_3OOH + CH_2CO + CH_3$	6.00×10^5	0.0	40.20
$c-C_3H_6O + C_2H_5 \leftrightarrow C_2H_5 + CH_2CO + CH_3$	6.00×10^5	0.0	46.02

356 (---) at higher conversions. When the two mechanisms are coupled with the Eley-Rideal propylene
 357 limit mechanism (M2), the amount of $c-C_3H_6O$ formed is appreciably reduced ($\Delta = -5.42\%$), with
 358 the selectivities to C_2H_4 ($\Delta = +0.22\%$), CO ($\Delta = +0.34\%$), and especially C_3H_6 ($\Delta = +3.95\%$)
 359 increasing accordingly as shown in Fig 8. The modification of the DTU mechanism therefore improves
 360 the agreement with experiment significantly. However, the discrepancies in $S(C_2H_4)$ and especially
 361 $S(CO)$ remain.

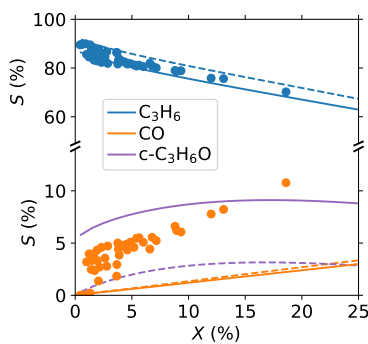


Figure 7: Effect of $c-C_3H_6O$ chemistry on the gas-phase selectivity vs conversion behaviour. The unmodified DTU mechanism (—) is compared to the DTU/B mechanism (---) containing $c-C_3H_6O$ formation and destruction pathways from Burluka et al.^[13] listed in Table 4. Same conditions as in Fig. 3

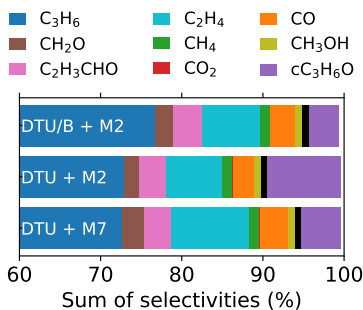
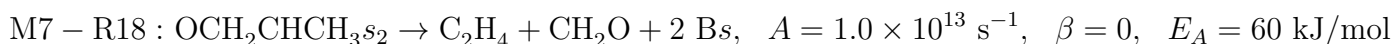
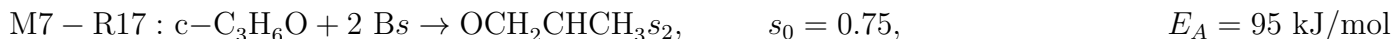


Figure 8: The effect of propylene oxide decomposition pathways on the selectivities. Shown for $V_{\text{bed}}/V_{\text{cat}} = 8.5$ at ~ 40 ml/min flow rate, with gas-phase and heterogeneous mechanisms as indicated.

362 A further possible explanation for the lack of experimentally observed $c\text{-C}_3\text{H}_6\text{O}$ may be due to its
 363 catalytic decomposition towards C–C scission products. Xiao and Wang investigated $c\text{-C}_3\text{H}_6\text{O}$ forma-
 364 tion pathways from propylene on Cu surfaces using density functional theory, proposing an oxygenated
 365 metallacyclic intermediate as the key intermediate.^[31] We note one of these intermediates could plausibly
 366 decompose towards CH_2O and C_2H_4 following a single H-shift and explore this possibility by augmenting
 367 the M2 mechanism by two speculative pathways denoted as M7.



368 The ring-opening adsorption of $c\text{-C}_3\text{H}_6\text{O}$ (M7-R17) is modelled as an associative process, requiring two
 369 sites, with a near-unity s_0 of 0.75 and a barrier height estimated from the energetics calculated for the
 370 Cu^0/Cu^+ couple (95 kJ/mol).^[31] The C–C bond scission and desorption are lumped into a single step
 371 (M7-R18), with an order-of-magnitude estimate of the pre-exponential, and the barrier height estimated
 372 from gas-phase endothermicity of the overall reaction (~ 60 kJ/mol). The results obtained when this
 373 mechanism is coupled to the original DTU gas phase chemistry (DTU + M7) are shown in Fig. 8.
 374 Sequence M7 significantly reduces the selectivity to $c\text{-C}_3\text{H}_6\text{O}$ ($\Delta = -4.27\%$) even at the highest bed
 375 dilution studied. This is compensated by an increase in $S(\text{C}_2\text{H}_4)$ ($\Delta = +2.75\%$), $S(\text{CO})$ ($\Delta = +0.83\%$),
 376 and $S(\text{CH}_2\text{O})$ ($\Delta = +0.69\%$) and suggests that discrepancies in selectivities between the gas-phase
 377 model and observed catalytic data may also arise from surface decomposition pathways.

378 3.8 Effect of higher flow rates

379 With increased inlet flow rates, the experimentally observed conversion drops and the selectivity shifts
380 towards C_3H_6 .^[8] This blow-off effect is more pronounced under higher dilutions of the catalytic bed, as
381 with $V_{bed}/V_{cat} = 8.5$ the selectivities to CO and CH_4 obtained at $\sim 40 \text{ ml min}^{-1}$ are almost double of
382 the selectivities at $\sim 160 \text{ ml min}^{-1}$. When the DTU/B mechanism is coupled with the Os-mediated
383 C_3H_6 mechanism (M2, — in Fig. 9), the experimental $X(C_3H_8)$ (\bullet) are well predicted at all studied
384 inlet flow rates and catalyst dilution ratios. Most qualitative trends with increasing flow rates are well
385 captured, including the shape of the blow-off in $S(C_2H_4)$, $S(CH_4)$, and $S(CO)$ at $V_{bed}/V_{cat} \geq 2.0$.
386 A notable exception is the slightly increasing $S(CH_4)$ (\bullet) with increased flow rate in the undiluted
387 case. Quantitatively, the agreement of the DTU/B + M2 mechanism with experimental selectivities is
388 poor, as experimental $S(C_3H_6)$ (\bullet) are overpredicted by the model (—) in all cases, with a maximum
389 absolute deviation ($\Delta_{max} = \max(S_{calc}(\text{prod}) - S_{exp}(\text{prod}))$) in $S(C_3H_6)$ of +9.6% (at $V_{bed}/V_{cat} = 3.5$,
390 120 ml min^{-1}). This leads to a significant underprediction in the C–C scission products even with an
391 undiluted catalyst. In section 3.5 we have coupled the DTU/B to the propyl-forming limit pathway (M4)
392 and we have obtained an excellent agreement in the undiluted case at 40 ml min^{-1} (see in Fig. 5).
393 However, as shown in Fig. 9, at higher inlet flow rates, the $S(C_2H_4)$ is overpredicted (....., $\Delta = +2.2\%$)
394 at the expense of $S(C_3H_6)$ (....., $\Delta = -6.3\%$). By contrast, in diluted cases with $V_{bed}/V_{cat} \geq 2.0$ this
395 combined mechanism struggles to predict the correct $S(CH_4)$ (.....) and $S(C_2H_4)$ at low inlet velocities,
396 with Δ_{max} in $S(C_2H_4) = -7.0\%$. Furthermore, $S(CO)$ (.....) remains significantly underpredicted. In
397 summary, the propylene forming limit mechanism (M2) captures the qualitative trends in selectivities
398 with bed dilution and flow rate, and is likely to be a key catalytic pathway. On the other hand,
399 the propyl limit mechanism (M4) produces results that are in better agreement with experiments in
400 undiluted beds, however upon dilution and at higher flow rates it is qualitatively inconsistent with the
401 experimental data. Hence we do not propose it as a credible catalytic pathway.

402 3.9 Effect of inlet O_2 and H_2O concentration

403 Venegas and coworkers have recently discussed the effects of varying inlet C_3H_8/O_2 ratio as well as the
404 impact H_2O co-feed has on the activity of the catalyst.^[9] Variation in the inlet C_3H_8/O_2 ratio has an

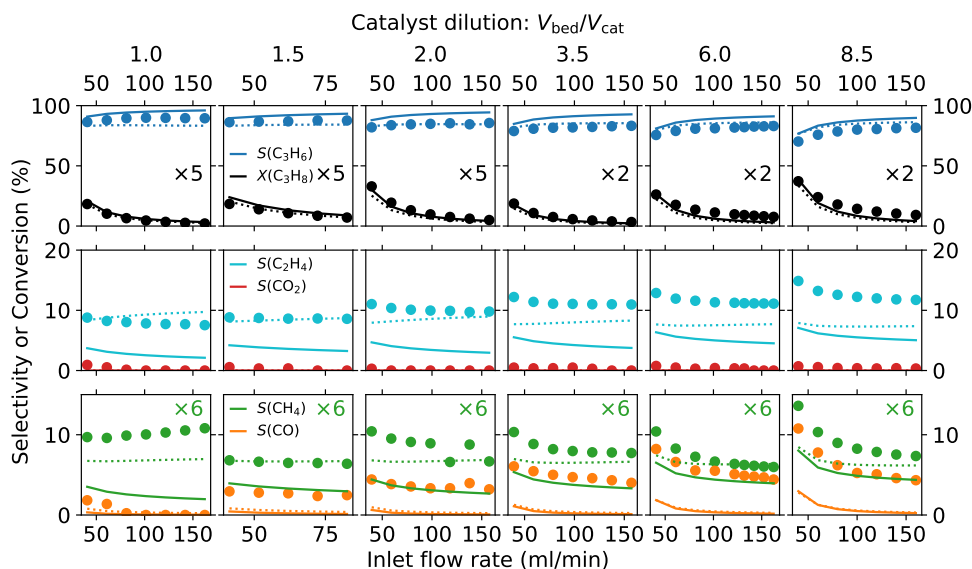


Figure 9: Selectivity and conversion of selected species as a function of inlet flow rate for all studied catalyst dilution ratios. Symbols are experimental data,^[8] lines are results calculated with the DTU/B gas-phase mechanism coupled either to the propane limit M2 (—) or the propyl limit M4 (.....) surface chemistries. Colour coding as per Fig. 5.

405 effect on selectivity, with higher amount of C_2 products observed at lower O_2 concentrations. On the
 406 other hand, co-feeding H_2O has almost no effect on selectivity, however the activity of the catalyst is
 407 increased significantly. The results are supported by density functional theory calculations, identifying
 408 a metastable active site that is formed dynamically under operating conditions. The authors propose
 409 the catalyst is responsible for activating oxygen, which then readily abstracts hydrogen from propane,
 410 yielding C_3H_7 radicals. This is at odds with our results above. Venegas and co-workers,^[9] propose
 411 that active sites can be regenerated in three ways: i) by recombination of surface hydroxyls followed
 412 by desorption of water yielding an empty site, ii) by reaction of surface hydroxyls with gas-phase water
 413 yielding an activated oxygen site, and iii) by reaction of surface hydrogens with gas-phase O_2 yielding
 414 peroxy radicals.

415 In the absence of a validated heterogeneous mechanism, we choose to investigate trends in selectivities
 416 caused by the changes in the inlet composition as predicted purely by gas-phase chemistry. To investigate
 417 the impact of the C_3H_8/O_2 ratio, we model the system as an adiabatic constant pressure reactor, allowing
 418 the inlet mixture to react from a starting temperature of $525^\circ C$, with a pressure of 1 atm, and a final
 419 $X(C_3H_8)$ set to 5% to allow a close comparison with the experimental data.^[9] The results are shown
 420 in Fig. 10. The agreement in $S(C_3H_6)$ and $S(CH_4)$ is excellent, the most significant discrepancy is the

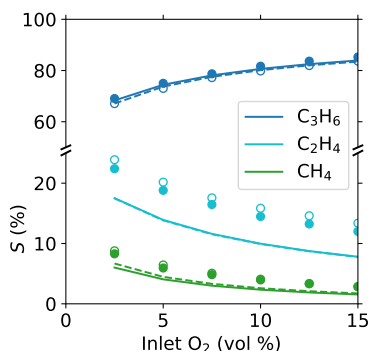


Figure 10: Selectivity to selected species as a function of inlet O_2 fraction. Symbols are experimental data, lines are results of calculations with the DTU/B mechanism. Showing cases with inlet C_3H_8 fraction of 15% (—, ●) and 25% (- - -, ○), inlet O_2 fraction on the abscissa, and N_2 as balance.

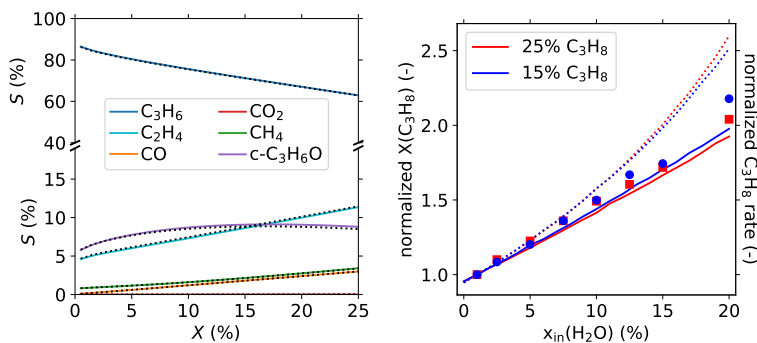


Figure 11: Effect of co-fed H_2O on gas-phase chemistry. Left: Gas-phase selectivity as a function of conversion, from adiabatic calculations, with dry feed (30% C_3H_8 , 15% O_2 , balance N_2 , —) and a feed containing 10% H_2O (.....). Right: Calculated gas-phase conversion of propane (lines) and experimental propane destruction rates (symbols)^[9] as a function of inlet fraction of H_2O , normalised by the 1% value. Results of isothermal (—) and adiabatic (.....) calculations for two mixtures (C_3H_8 and H_2O as indicated, 15% O_2 , balance N_2). All calculations performed with the DTU/B gas-phase mechanism.

421 underprediction in $S(C_2H_4)$ (—, $\Delta_{max} = -6.4\%$). The underprediction remains roughly constant at
 422 all inlet O_2 and is comparable to the results shown in Fig. 3. Therefore, the changes in selectivities upon
 423 variation in the C_3H_8/O_2 ratio can be attributed to the gas-phase chemistry.

424 The changes in the activity of the system with inlet mixtures that include water are two-fold: there is
 425 an immediate spike in the activity upon addition of water, accompanied by a smaller and gradual increase
 426 in activity while water is co-fed. Addition of water does not impact selectivity.^[9] Our calculations result
 427 in a 20% faster ignition for a mixture containing water (30% C_3H_8 , 15% O_2 , 10% H_2O , balance N_2)
 428 compared to the dry inlet composition at 500°C. As shown in Fig. 11(left), the calculated selectivity
 429 profiles as a function of conversion are unchanged. The relationship between ignition delay time and
 430 conversion is not straightforward. If we assume the residence time is dictated by the inlet flow rate and

oven temperature, and therefore constant with respect to the inlet composition, we can calculate the residence time required to obtain a nominal conversion for a dry case, and use this value to compare the relative increase in gas-phase activity due to water addition. Experimental activity data from inlet mixtures of 25% or 15% C_3H_8 , 15% O_2 , and 1–20% H_2O (balance is N_2) is available for a constant inlet flow rate with a nominal conversion of 3%.^[9] The results of adiabatic (·····) and isothermal (—) gas-phase calculations, starting at the experimental temperature of 525°C, are shown in Fig. 11(right). The experimental results are in excellent agreement with the isothermal calculations at inlet fractions of H_2O below 10%. Above this value the experiments begin to approach the adiabatic limit, likely as a consequence of the heat release caused by ODH. We may therefore conclude that the experimentally observed immediate increase in the activity in cases with co-fed water can be adequately explained by gas-phase phenomena. The smaller, gradual effect may also be caused by an additional release of water. However, such transient effects can not be account for using steady-state modelling, especially without an experimental determination of the amount of water in the product stream.

4 Summary and outlook

The current work corroborates the hypothesis^[6,8,10] that gas-phase chemistry is the main driver of the catalytic performance of hBN as a selective catalyst for ODH of propane. The hBN surface acts as a driver of conversion, however the influence of the surface chemistry on the resulting product distribution decreases significantly with dilution of the catalytic bed, as gas-phase effects begin to dominate. The work highlights the necessity of modelling of the whole heated section of the reactor: even if little to no conversion is observed in blank experiments, and best practices to limit post-catalytic combustion are followed, we show the post-catalytic zone can be responsible for up to 50% of the total observed conversion.

The propylene limit heterogeneous mechanism featuring the Eley-Rideal mediated propylene forming limit (M2) coupled with the DTU mechanism^[11] augmented by propylene oxide pathways from Burluka et al.^[13] (DTU/B) is able to qualitatively predict the experimentally observed propane conversion as well as most trends in selectivities as a function of catalyst dilution and inlet flow rate. A contribution of secondary catalytic pathways is likely necessary to quantitatively reproduce the experimentally ob-

458 served $C_2:C_1$ product ratio in undiluted beds. However, upon dilution of the catalytic bed all six limit
459 mechanisms converge towards the gas-phase limit, which leads to an underprediction in both $S(C_2H_4)$
460 and $S(CO)$ even if those products are formed on the catalyst. The DTU mechanism^[11] predicts the
461 formation of a significant amount of propylene oxide, and to a lesser extent acrolein and formaldehyde.
462 The overprediction of propylene oxide is most likely a mechanistic artefact due to missing decomposition
463 pathways or catalytic activity of hBN towards $c-C_3H_6O$. The modified DTU/B mechanism is able to
464 predict the observed effects of inlet C_3H_8/O_2 ratio on selectivities, and can account for the immediate
465 increase in activity upon H_2O co-feed. The $C_3:C_2:C_1$ product distribution predicted using the modified
466 DTU/B mechanism matches the experimentally observed distribution, however, the detailed speciation,
467 particularly of C_1 oxygenated species, is at odds with the modelled experiments. Further study of the
468 low-temperature oxidation chemistry of the above species is necessary.

469 Finally, we would like to emphasise the importance of a comprehensive approach to the evaluation
470 of gas-phase kinetics in any mechanistic study involving heterogeneous phenomena at elevated temper-
471 atures. One of the key advantages of microkinetics over the Langmuir-Hinshelwood-Hougen-Watson
472 model is the ease with which gas-phase and heterogeneous models of various complexities can be cou-
473 pled. With open-source solvers, such as Cantera,^[12] the tools are available to everyone; we hope that
474 the executable code archive attached in the Supporting information may encourage wider adoption of
475 such approaches in the catalytic community.

476 Acknowledgment

477 The authors would like to thank Prof. Ivo Hermans for valuable comments. PK would like to thank the
478 Forrest Research Foundation for funding.

479 Supporting information

480 Supporting information available. The complete code archive including all calculations, parameter
481 fitting, and plotting scripts is available on Zenodo under DOI: 10.5281/zenodo.4106081. The archive
482 is arranged in a Binder-executable format, see <https://mybinder.org/v2/zenodo/10.5281/zenodo>.

484 **References**

- 485 [1] J. T. Grant, C. A. Carrero, F. Goeltl, J. Venegas, P. Mueller, S. P. Burt, S. E. Specht, W. P. McDermott,
486 A. Chiericato, and I. Hermans, "Selective oxidative dehydrogenation of propane to propene using boron
487 nitride catalysts," *Science*, vol. 354, pp. 1570–1573, Dec. 2016.
- 488 [2] L. Shi, D. Wang, W. Song, D. Shao, W.-P. Zhang, and A.-H. Lu, "Edge-hydroxylated boron nitride for
489 oxidative dehydrogenation of propane to propylene," *ChemCatChem*, vol. 9, pp. 1788–1793, May 2017.
- 490 [3] C. A. Carrero, R. Schloegl, I. E. Wachs, and R. Schomaecker, "Critical literature review of the kinetics
491 for the oxidative dehydrogenation of propane over well-defined supported vanadium oxide catalysts," *ACS*
492 *Catal.*, vol. 4, pp. 3357–3380, Oct. 2014.
- 493 [4] P. Chaturbudy, M. Ahamed, and M. Eswaramoorthy, "Oxidative dehydrogenation of propane over a high
494 surface area boron nitride catalyst: Exceptional selectivity for olefins at high conversion," *ACS Omega*,
495 vol. 3, pp. 369–374, Jan. 2018.
- 496 [5] J. T. Grant, W. P. McDermott, J. M. Venegas, S. P. Burt, J. Micka, S. P. Phivilay, C. A. Carrero,
497 and I. Hermans, "Boron and boron-containing catalysts for the oxidative dehydrogenation of propane,"
498 *ChemCatChem*, vol. 9, pp. 3623–3626, Oct. 2017.
- 499 [6] J. M. Venegas, W. P. McDermott, and I. Hermans, "Serendipity in Catalysis Research: Boron-Based
500 Materials for Alkane Oxidative Dehydrogenation," *Acc. Chem. Res.*, vol. 51, pp. 2556–2564, Oct. 2018.
- 501 [7] L. Shi, D. Wang, and A.-H. Lu, "A viewpoint on catalytic origin of boron nitride in oxidative dehydro-
502 genation of light alkanes," *Chinese Journal of Catalysis*, vol. 39, pp. 908–913, May 2018.
- 503 [8] J. M. Venegas and I. Hermans, "The influence of reactor parameters on the boron nitride-catalyzed oxida-
504 tive dehydrogenation of propane," *Org. Process Res. Dev.*, vol. 22, pp. 1644–1652, Dec. 2018.
- 505 [9] J. M. Venegas, Z. Zhang, T. O. Agbi, W. P. McDermott, A. Alexandrova, and I. Hermans, "Why boron
506 nitride is such a selective catalyst for the oxidative dehydrogenation of propane," *Angew. Chem. Int. Ed.*,
507 p. 9, 2020.
- 508 [10] W. P. McDermott, J. Venegas, and I. Hermans, "Selective oxidative cracking of *n*-butane to light olefins
509 over hexagonal boron nitride with limited formation of CO_x," *ChemSusChem*, vol. 13, pp. 152–158, Jan.
510 2020.
- 511 [11] H. Hashemi, J. M. Christensen, L. B. Harding, S. J. Klippenstein, and P. Glarborg, "High-pressure oxida-
512 tion of propane," *Proceedings of the Combustion Institute*, vol. 37, no. 1, pp. 461–468, 2019.
- 513 [12] D. G. Goodwin, R. L. Speth, H. K. Moffat, and B. W. Weber, "Cantera: An object-oriented software
514 toolkit for chemical kinetics, thermodynamics, and transport processes." Zenodo, Aug. 2018.
- 515 [13] A. Burluka, M. Harker, H. Osman, C. Sheppard, and A. Konnov, "Laminar burning velocities of three
516 C₃H₆O isomers at atmospheric pressure," *Fuel*, vol. 89, pp. 2864–2872, Oct. 2010.
- 517 [14] H. Wang, E. Dames, B. Sirjean, D. A. Sheen, R. Tango, A. Violi, J. Y. W. Lai, F. N. Egolfopoulos, D. F.
518 Davidson, R. K. Hanson, C. T. Bowman, C. K. Law, W. Tsang, N. P. Cernansky, D. L. Miller, and R. P.
519 Lindstedt, "A high-temperature chemical kinetic model of *n*-alkane (up to *n*-dodecane), cyclohexane, and
520 methyl-, ethyl-, *n*-propyl and *n*-butyl-cyclohexane oxidation at high temperatures, JetSurF version 2.0,"
521 Sept. 2010.

- 522 [15] C. F. Goldsmith, W. H. Green, and S. J. Klippenstein, "Role of $O_2 + QOOH$ in low-temperature ignition of
523 propane. 1. Temperature and pressure dependent rate coefficients," *J. Phys. Chem. A*, vol. 116, pp. 3325–
524 3346, Apr. 2012.
- 525 [16] R. Sivaramakrishnan, M.-C. Su, J. V. Michael, S. J. Klippenstein, L. B. Harding, and B. Ruscic, "Shock
526 Tube and Theoretical Studies on the Thermal Decomposition of Propane: Evidence for a Roaming Radical
527 Channel," *J. Phys. Chem. A*, vol. 115, pp. 3366–3379, Apr. 2011.
- 528 [17] R. Sivaramakrishnan, N. Srinivasan, M.-C. Su, and J. Michael, "High temperature rate constants for $OH+$
529 alkanes," *Proceedings of the Combustion Institute*, vol. 32, no. 1, pp. 107–114, 2009.
- 530 [18] H. Wang, X. You, A. V. Joshi, S. G. Davis, A. Laskin, F. N. Egolfopoulos, and C. K. Law, "USC Mech
531 Version II. High-temperature combustion reaction model of $H_2/CO/C_1-C_4$ compounds.," May 2007.
- 532 [19] S. S. Merchant, C. F. Goldsmith, A. G. Vandeputte, M. P. Burke, S. J. Klippenstein, and W. H. Green,
533 "Understanding low-temperature first-stage ignition delay: Propane," *Combustion and Flame*, vol. 162,
534 pp. 3658–3673, 2015.
- 535 [20] O. Deutschmann, R. Schmidt, F. Behrendt, J. Warnatz, and J. Warnat, "Numerical modeling of catalytic
536 ignition," *Proc. Combust. Inst.*, vol. 26, no. 1, pp. 1747–1754, 1996.
- 537 [21] J. Sheng, B. Yan, W.-D. Lu, B. Qiu, X.-Q. Gao, D. Wang, and A.-H. Lu, "Oxidative dehydrogenation of
538 light alkanes to olefins on metal-free catalysts," *Chem. Soc. Rev.*, vol. 50, no. 2, pp. 1438–1468, 2021.
- 539 [22] A. M. Love, B. Thomas, S. E. Specht, M. P. Hanrahan, J. M. Venegas, S. P. Burt, J. T. Grant, M. C.
540 Cendejas, W. P. McDermott, A. J. Rossini, and I. Hermans, "Probing the transformation of boron nitride
541 catalysts under oxidative dehydrogenation conditions," *J. Am. Chem. Soc.*, vol. 141, pp. 182–190, Jan.
542 2019.
- 543 [23] R. W. Dorn, M. C. Cendejas, K. Chen, I. Hung, N. R. Altvater, W. P. McDermott, Z. Gan, I. Hermans, and
544 A. J. Rossini, "Structure determination of boron-based oxidative dehydrogenation heterogeneous catalysts
545 with ultrahigh field 35.2 T ^{11}B solid-state NMR spectroscopy," *ACS Catal.*, vol. 10, pp. 13852–13866, Dec.
546 2020.
- 547 [24] Z. Zhang, E. Jimenez-Izal, I. Hermans, and A. N. Alexandrova, "Dynamic phase diagram of catalytic
548 surface of hexagonal boron nitride under conditions of oxidative dehydrogenation of propane," *J. Phys.*
549 *Chem. Lett.*, vol. 10, pp. 20–25, Jan. 2019.
- 550 [25] P. Kraus and R. P. Lindstedt, "Microkinetic mechanisms for partial oxidation of methane over platinum
551 and rhodium," *J. Phys. Chem. C*, vol. 121, pp. 9442–9453, May 2017.
- 552 [26] V. R. Tarnawski, T. Momose, and W. H. Leong, "Thermal conductivity of standard sands II. Saturated
553 conditions," *Int J Thermophys*, vol. 32, pp. 984–1005, May 2011.
- 554 [27] S. L. Shindé and J. Goela, *High thermal conductivity materials*. New York: Springer, 2006.
- 555 [28] G. Magnani, S. Galvagno, G. Sico, S. Portofino, C. Freda, and E. Burresti, "Sintering and mechanical
556 properties of β -SiC powder obtained from waste tires," *J Adv Ceram*, vol. 5, pp. 40–46, Mar. 2016.
- 557 [29] J. A. Loiland, Z. Zhao, A. Patel, and P. Hazin, "Boron-containing catalysts for the oxidative dehydrogena-
558 tion of ethane/propane mixtures," *Ind. Eng. Chem. Res.*, vol. 58, pp. 2170–2180, Feb. 2019.
- 559 [30] D. A. Knyazkov, A. M. Dmitriev, O. P. Korobeinichev, K. N. Osipova, G. Pio, A. G. Shmakov, and
560 E. Salzano, "Structure of premixed flames of propylene oxide: Molecular beam mass spectrometric study
561 and numerical simulation," *Proceedings of the Combustion Institute*, p. S1540748920304296, Sept. 2020.

- 562 [31] T.-T. Xiao and G.-C. Wang, “A DFT and microkinetic study of propylene oxide selectivity over copper-
563 based catalysts: effects of copper valence states,” Catal. Sci. Technol., vol. 10, no. 22, pp. 7640–7651,
564 2020.
- 565 [32] Z. Kalenik and E. E. Wolf, “The role of gas-phase reactions during methane oxidative coupling,” in Methane
566 Conversion by Oxidative Processes: Fundamental and Engineering Aspects, Van Nostrand Reinhold Catal-
567 ysis Series, p. 548, Springer Science & Business Media, 2013.
- 568 [33] G. Shangpeng, “Crystal structures and band gap characters of h-BN polytypes predicted by the dispersion
569 corrected DFT and GW method,” Solid State Communications, vol. 152, pp. 1817–1820, 2012.
- 570 [34] M. Hartmann, L. Maier, H. Minh, and O. Deutschmann, “Catalytic partial oxidation of iso-octane over
571 rhodium catalysts: An experimental, modeling, and simulation study,” Combustion and Flame, vol. 157,
572 pp. 1771–1782, Sept. 2010.
- 573 [35] X. Rozanska, R. Fortrie, and J. Sauer, “Oxidative Dehydrogenation of Propane by Monomeric Vanadium
574 Oxide Sites on Silica Support,” J. Phys. Chem. C, vol. 111, pp. 6041–6050, Apr. 2007.
- 575 [36] L. Shi, Y. Wang, B. Yan, W. Song, D. Shao, and A.-H. Lu, “Progress in selective oxidative dehydrogenation
576 of light alkanes to olefins promoted by boron nitride catalysts,” Chem. Commun., vol. 54, no. 78, pp. 10936–
577 10946, 2018.
- 578 [37] J. Tian, J. Tan, M. Xu, Z. Zhang, S. Wan, S. Wang, J. Lin, and Y. Wang, “Propane oxidative dehydro-
579 genation over highly selective hexagonal boron nitride catalysts: The role of oxidative coupling of methyl,”
580 Sci. Adv., vol. 5, p. eaav8063, Mar. 2019.
- 581 [38] A. Lifshitz and C. Tamburu, “Isomerization and decomposition of propylene oxide. Studies with a single-
582 pulse shock tube,” J. Phys. Chem., vol. 98, pp. 1161–1170, Jan. 1994.